Defect detection in monocrystalline silicon wafers using high frequency guided waves

Cite as: AIP Conference Proceedings **2102**, 020013 (2019); https://doi.org/10.1063/1.5099717
Published Online: 08 May 2019

Bernard Masserey, Mathieu Simon, Jean-Luc Robyr, and Paul Fromme

Defect Detection in Monocrystalline Silicon Wafers Using High Frequency Guided Waves

Bernard Masserey[1], Mathieu Simon[1], Jean-Luc Robyr[1], Paul Fromme[2a]

[1] *Department of Mechanical Engineering, University of Applied Sciences, Fribourg, Switzerland*
[2] *Department of Mechanical Engineering, University College London, WC1E 7JE, UK*

[a)]Corresponding author: p.fromme@ucl.ac.uk

Abstract. Monocrystalline silicon wafers are employed in the photovoltaic industry for the manufacture of solar panels with high conversion efficiency. Micro-cracks can be induced in the thin wafer surfaces during the cutting process. High frequency guided waves are considered for the testing of the wafers and the nondestructive characterization of the micro-cracks. Experimentally selective excitation of the fundamental Lamb wave modes was achieved using a custom-made angle beam transducer and holder to achieve a controlled contact pressure. The out-of-plane component of the guided wave propagation was measured using a noncontact laser interferometer, scanned parallel to the specimen surface using a positioning system. The material anisotropy of the monocrystalline silicon leads to variations of the guided ultrasonic wave characteristics depending on the propagation direction relative to the monocrystalline silicon orientation. In non-principal directions of the crystal, wave beam skewing occurs due to material anisotropy. Artificial defects were introduced in the wafers using a micro indenter with varying force. The defects were characterized from microscopy images to measure the indent depth and combined crack lengths. The scattering of the A_0 Lamb wave mode was measured experimentally. The scattered wave field showed high amplitude peaks close to the defect location and an interference pattern indicative of a scattered wave, but was found to be not symmetric to the defect and crystallographic orientations. Characteristics of the scattered wave amplitudes were correlated to the defect size and the detection sensitivity discussed.

Keywords: Monocrystalline Silicon, Lamb Waves, Scattering, Ultrasonics
PACS: 43.20.Mv, 43.35.Zc, 43.35.Cg

INTRODUCTION

Solar panels provide an important contribution to renewable electricity generation. They often contain monocrystalline silicon wafers, with thinner wafers increasing conversion efficiency and lowering production costs. The minimum practical thickness is limited by small cracks introduced during the cutting process, which can lead to wafer breakage during handling and in-service due to mechanical and thermal stresses [1]. Different non-destructive evaluation (NDE) techniques have been investigated for defect detection in silicon wafers, e.g. thermography, impact testing, ultrasonic waves, and photo-luminescence imaging [2, 3]. Guided waves have the required long propagation distance compared to the plate thickness and thus full area coverage for efficient in-process monitoring and defect detection [4, 5]. Hidden damage [6, 7] and fatigue cracks [8, 9] can be detected with good sensitivity using high frequency guided waves. Crack detection in silicon wafers was achieved using laser excitation and measurement of the fundamental guided wave modes [10]. Cracks in monocrystalline and polycrystalline silicon wafers were detected using air-coupled transducers in a B-scan configuration [11]. The guided wave scattering pattern depends on the crack orientation and dimensions compared to the wavelength [12].

For anisotropic materials, the energy focusing of longitudinal and transverse ultrasonic waves can be theoretically predicted [13] and scattering at defects investigated [14]. The direction dependency of the velocity in silicon plates was measured and compared to theory [15]. Material properties can be obtained from the experimental results [16]. Using a line laser source, the zero-group velocity (ZGV) of guided waves in silicon wafers was measured, to obtain the direction dependency due to stiffness variation [17]. The variation in guided wave arrival time and amplitude with propagation direction was studied [18].

45th Annual Review of Progress in Quantitative Nondestructive Evaluation, Volume 38
AIP Conf. Proc. 2102, 020013-1–020013-8; https://doi.org/10.1063/1.5099717
Published by AIP Publishing. 978-0-7354-1832-5/$30.00

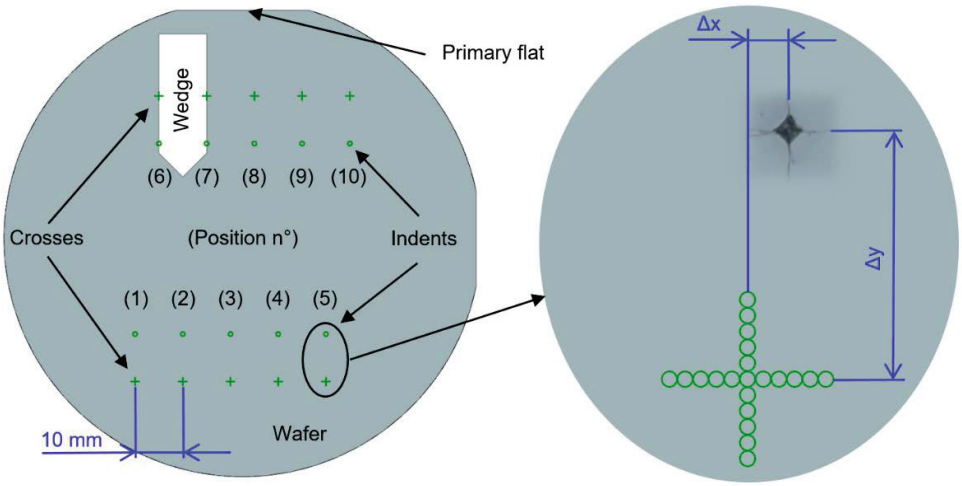

FIGURE 1. Left: schematic of silicon wafer with defect and wedge transducer positions marked; right: surface-printed crosses behind each indent location for localization of defect for measurements.

The angular dependency of guided wave propagation in thin monocrystalline silicon wafers was previously investigated experimentally and compared to Finite Element (FE) simulations [19, 20]. Significant wave skewing and widening due to the anisotropy was observed [21]. The fundamental A_0 guided wave mode was excited using a custom-made wedge transducer and measured using a non-contact laser interferometer. For this contribution the near-field scattering at artificial surface defects (indent and cracks) was investigated for different defect dimensions to obtain a better understanding of the sensitivity of guided waves.

SILICON WAFERS WITH DEFECTS

The specimens were boron doped monocrystalline silicon wafers with <100> crystallographic orientation, 100 mm diameter and 380 µm nominal thickness (Fig. 1). Artificial surface defects were introduced by making an indent with a specified force (1, 2, 3, 4 N) and controlled speed. This led to an indent of controlled size and depth, and generated cracks at the four corners aligned along the <110> direction as shown in Fig. 2 (left). Especially for the higher indent forces, chipping of the silicon wafer was observed as shown in Fig. 2 (right). These were not investigated, and sufficient indents were created to obtain at least 3 indents without significant chipping at each force level. The indent and overall defect size were measured optically using a microscope. The defect size shows a good, linear correlation with the indent force with some limited variation for each force level.

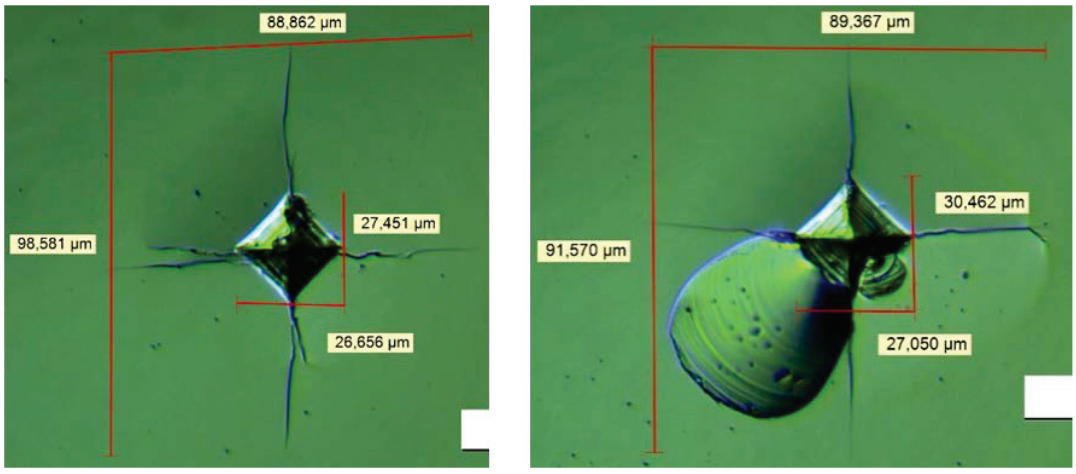

FIGURE 2. Optical microscopy images of indent and surface cracks with measured dimensions; left: indent without chipping; right: indent with chipping.

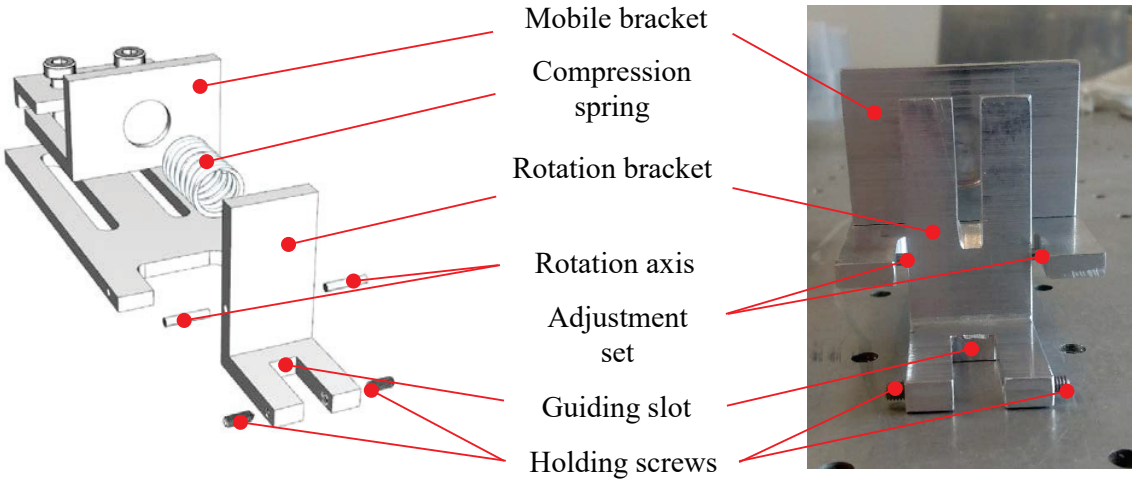

FIGURE 3. Schematic representation (left) and photograph (right) of wedge transducer holder.

GUIDED WAVE EXPERIMENTS

The wafers were fixed by a custom-made wafer and wedge holder (Fig. 3, 4) to reduce the risk of wafer breakage. The fundamental A_0 guided wave mode was selectively excited using a custom-made nylon wedge (41° angle) with a commercial piezoelectric transducer. The excitation signal was a narrowband sinusoidal pulse (12 cycles in a Hanning window) with a center frequency of 5 MHz. The signal was defined using Labview, generated using an arbitrary function generator, amplified using a power amplifier, and applied to the angle beam transducer. The out-of-plane surface displacement was measured using a non-contact commercial laser interferometer, positioned using a scanning rig. The measured voltage signal was frequency filtered (bandpass: 2-8 MHz), averaged (40 averages) and transferred from the oscilloscope to the PC for evaluation. The measurement grid around the defect was 400 µm by 400 µm with a step size of 5 µm in both directions to accurately capture local variations in the scattered wave field. The amplitude at each point of the measurement grid was evaluated using the maximum amplitude of the envelope (Hilbert transform) of the measured time trace.

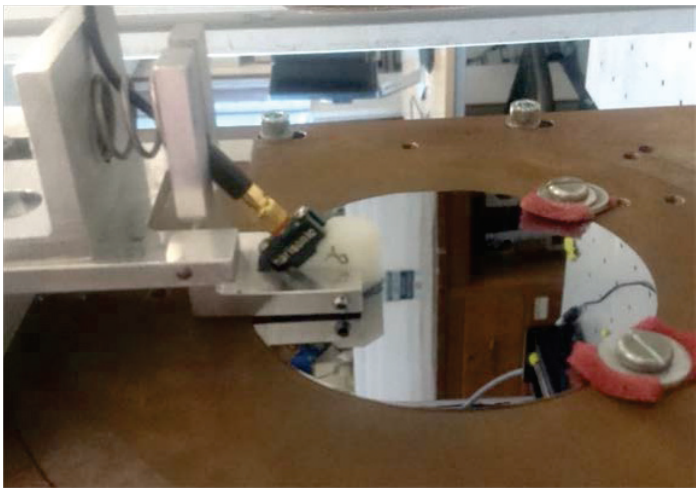

FIGURE 4. Photograph of silicon wafer fixed on holder with wedge transducer.

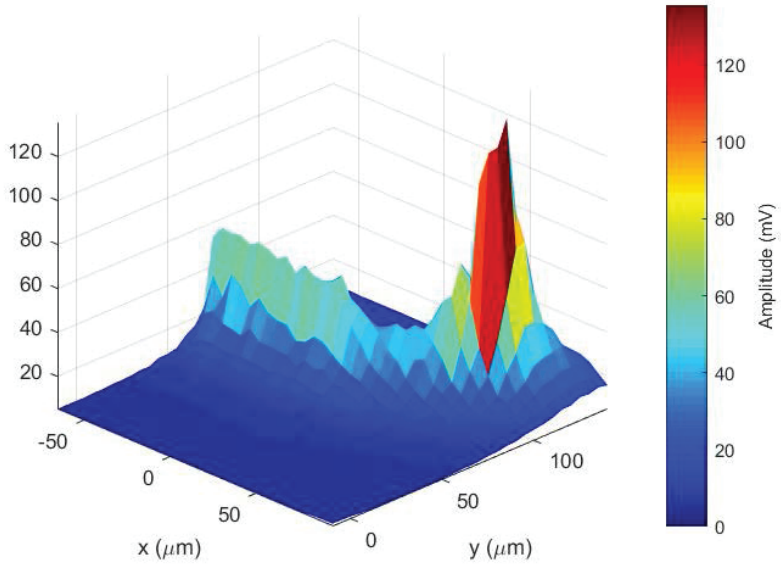

FIGURE 5. Measured noise due to laser reflection on damaged surface, standard deviation of signal measured without ultrasonic excitation (no filter, no average), 5 µm step size.

Several steps were required to center the laser measurement on the exact defect location. Behind each indent a cross had been surface-printed onto the wafer and the distance to the indent recorded optically when the indents were made (Fig. 1). These were used as the starting point and the laser interferometer positioned relative to the cross by observing the laser reflection. The scan rig was then moved to the recorded defect position and an initial scan performed to exactly center the measurement area. With a step size of 5 µm the noise in the measured signal without ultrasonic excitation was recorded (no filter, no average) and the standard deviation of each recorded time trace calculated (Fig. 5). This was indicative of the quality of the laser beam reflection on the wafer surface and provided an accurate indication of the indent location as the area of highest noise. This allowed the generation of composite pictures as shown in Fig. 6, showing the scattered guided wave field amplitude overlaid with the microscopy image of the defect and isolines to indicate the areas of higher measurement noise. It should be noted that the accuracy of the relative positioning has not been verified independently.

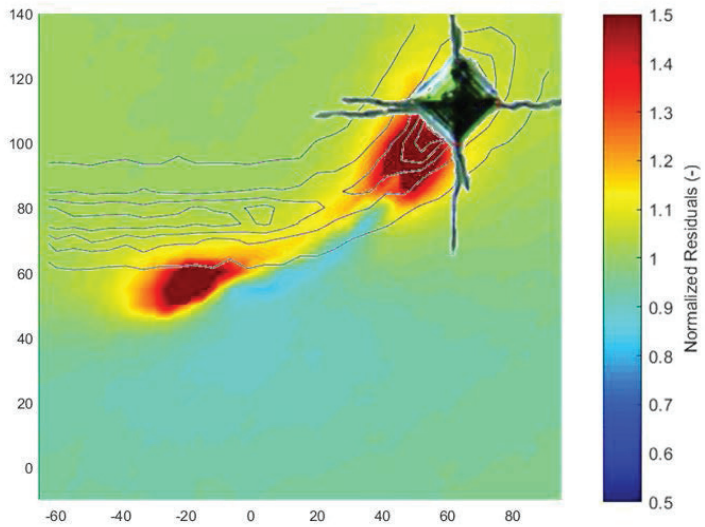

FIGURE 6. Composite image of measured scattered wave field (normalized amplitude shown color-coded), measured noise (isolines), overlaid with optical microscopy image of defect (indent and cracks) at location of highest noise.

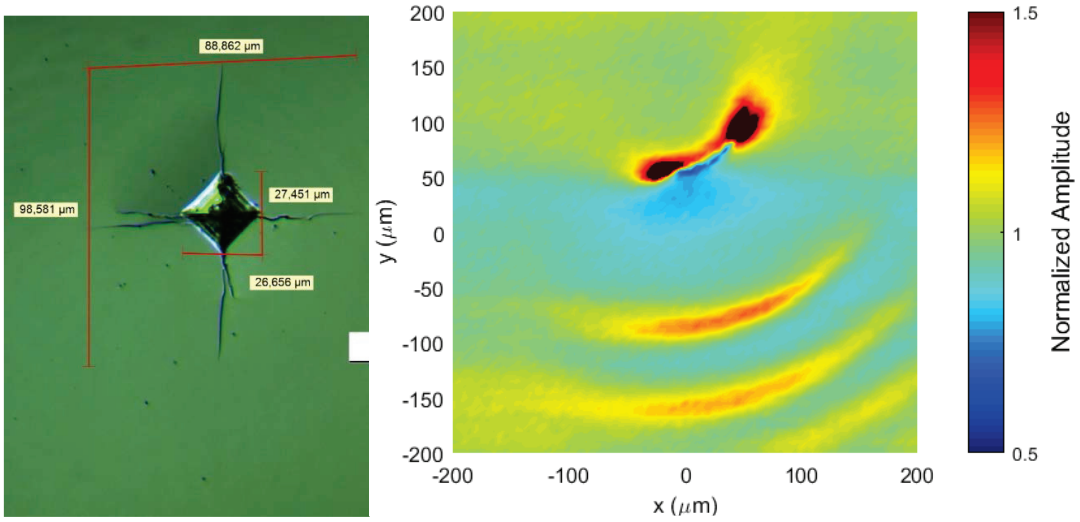

FIGURE 7. Left: Optical microscopy of defect for 4 N indent force; right: measured guided wave scattered field, normalized with incident wave amplitude, A_0 mode at 5 MHz center frequency, step size 5 µm.

MEASURED SCATTERED WAVE FIELDS

The wave fields were measured around 3 defects for each indent force and one is shown for each force level. Fig. 7 shows the optical microscopy image and the scattered wave field for the largest indent force of 4 N. Using the geometry of the pyramid shaped indenter (opening angle: 136°), an indent depth of 5 µm can be calculated based on the diagonal size of the indent of approximately 27 µm. The cracks from the 4 corners of the indent are aligned along the <110> directions with an overall size of approximately 90-100 µm for this force level. The scattered wave amplitude field (Fig. 7 right) has the incident wave propagation direction along the y-axis (bottom to top). The scattered wave field does not show the expected symmetry, but appears to be angled towards the right. Close to the location of the defect two significant peaks can be observed with a maximum amplitude of more than twice the incident wave amplitude (normalized). The two peaks are approximately 100 µm apart and an area of low amplitude is visible before the defect. Further in the negative y-direction an interference pattern with semi-circular areas of high and low amplitude indicates constructive and destructive interference between the incident wave and the scattered wave. The scattered wave fields for defects due to an indent force of 3 N are reasonably similar, with a typical microscopy image and scattered field shown in Fig. 8. Defects had an overall size of about 75 µm and the indent depth was estimated as 4 µm.

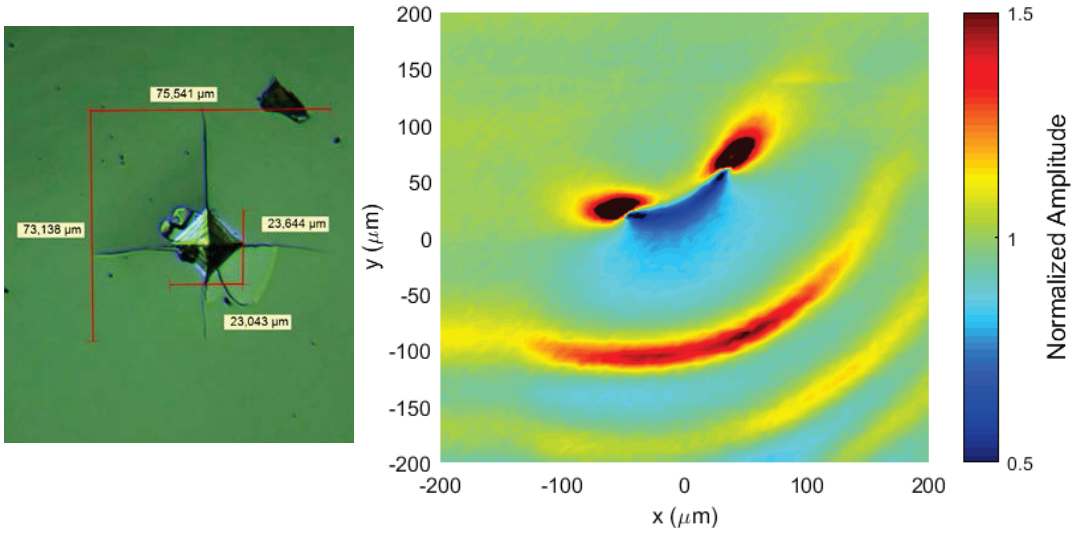

FIGURE 8. Left: Optical microscopy of defect for 3 N indent force; right: measured guided wave scattered field, normalized with incident wave amplitude, A_0 mode at 5 MHz center frequency, step size 5 µm.

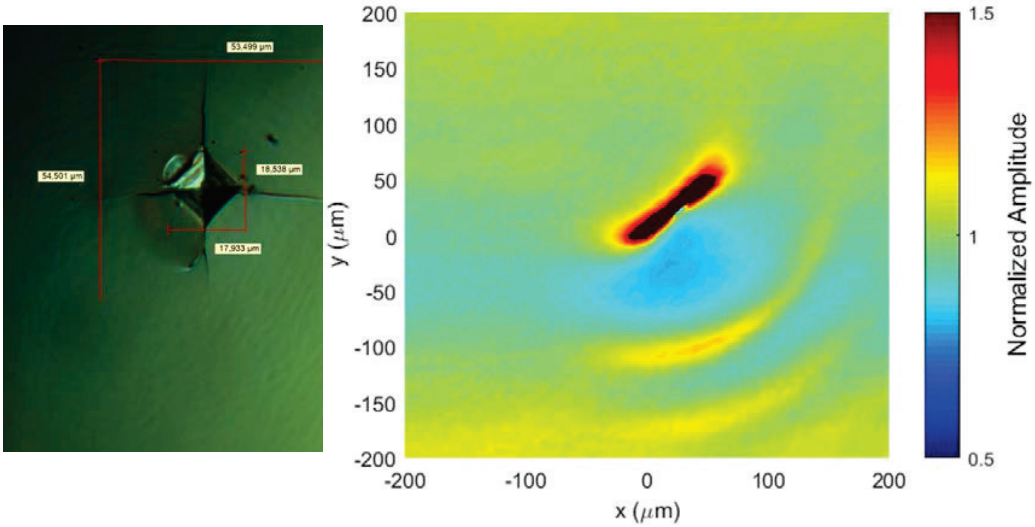

FIGURE 9. Left: Optical microscopy of defect for 2 N indent force; right: measured guided wave scattered field, normalized with incident wave amplitude, A_0 mode at 5 MHz center frequency, step size 5 µm.

For the defect with an indent force of 2 N (Fig. 9), the overall defect size was approximately 50 µm and the indent depth was calculated as 3 µm. For these smaller defects, it appeared that the two peaks merged to a single peak, albeit of similar high amplitude. Again, an area of low amplitude and a semi-circular interference pattern can be seen. For the lowest indent force of 1 N (Fig. 10), the defect size was approximately 30 µm and the indent depth 2 µm. For these defect, no significant amplitude peak could be observed, with significantly lower maximum amplitude than for the larger defects. However, a clear semi-circular interference pattern could still be seen with similar dimensions to the other scattered fields but lower amplitude.

GUIDED WAVE SCATTERED FIELD EVALUATION

For the 12 defects, the maximum amplitude of the scattered wave pattern was extracted from the scattered field, normalized with the amplitude of the incident wave for each measurement. For most defects, this was one of the amplitude peaks visible close to the defect. Therefore, some uncertainty due the spatial sampling of such a singularity with a step size of 5 µm exists. The maximum amplitudes are shown in Fig. 11 against the optically measured defect size (indent and cracks combined) perpendicular to the incident wave propagation direction. For the larger defects a very high amplitude can be observed.

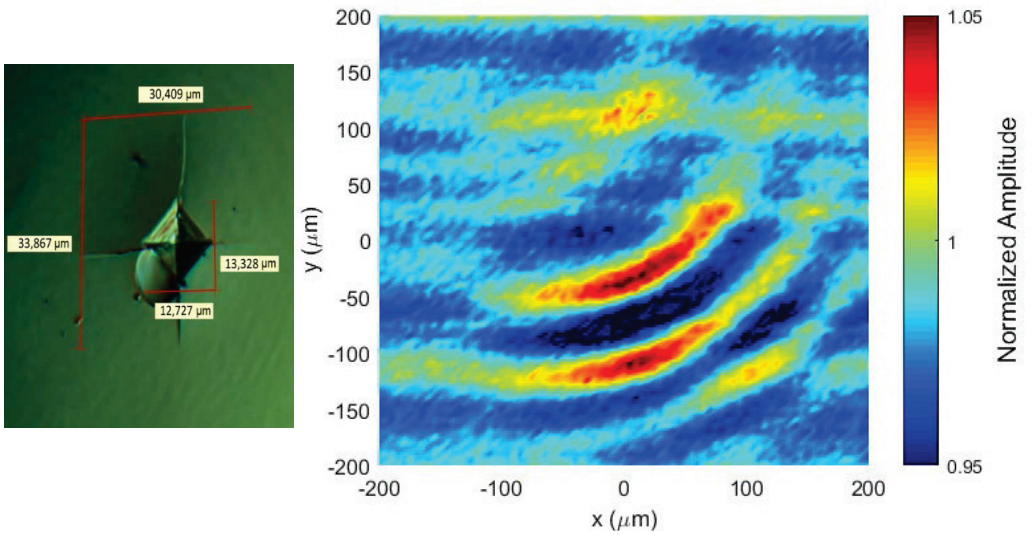

FIGURE 10. Left: Optical microscopy of defect for 1 N indent force; right: measured guided wave scattered field, normalized with incident wave amplitude, A_0 mode at 5 MHz center frequency, step size 5 µm.

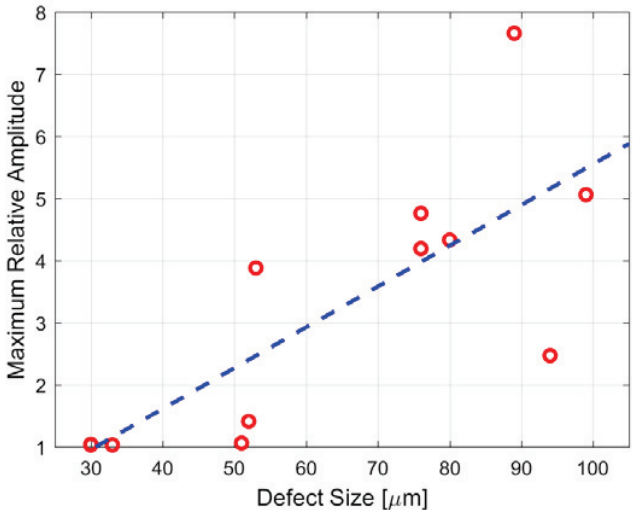

FIGURE 11. Maximum amplitude of measured guided wave scattered field (normalized with incident wave), against optically measured defect size (perpendicular to incident wave, indent and cracks combined); dashed line: linear fit to measured amplitude values.

For the smallest defects the maximum scattered amplitude is only about 5-10% of the incident wave amplitude but can still be observed clearly. From a linear fit (dashed line) some correlation of the maximum scattered amplitude values with overall defect size can be observed, but due to the singularity of the amplitude peaks, the correlation is limited. For the smallest defects, a significantly lower scattered wave amplitude was observed.

In order to avoid the singularity of the amplitude peaks close to the defect location, the amplitude of the scattered wave interference was evaluated and is shown in Fig. 12 against the overall defect size. For all defects (except one) the scattered wave field showed an interference pattern with semi-circular areas of high and low amplitudes. The patterns were not symmetric to the incident wave direction but showed a consistent radius of the innermost semi-circle of high amplitude of approximately 200 µm, a quarter of the wavelength of the A_0 mode. The amplitude should therefore provide some indication of the magnitude of any scattered waves. Fig. 12 again shows a clear increase in amplitude with overall defect size, but a rather large variation as compared to a linear fit (dashed line). For the largest defects a scattered amplitude of up about half the amplitude of the incident wave was observed, making it likely that such defects could be detected from a stand-off distance.

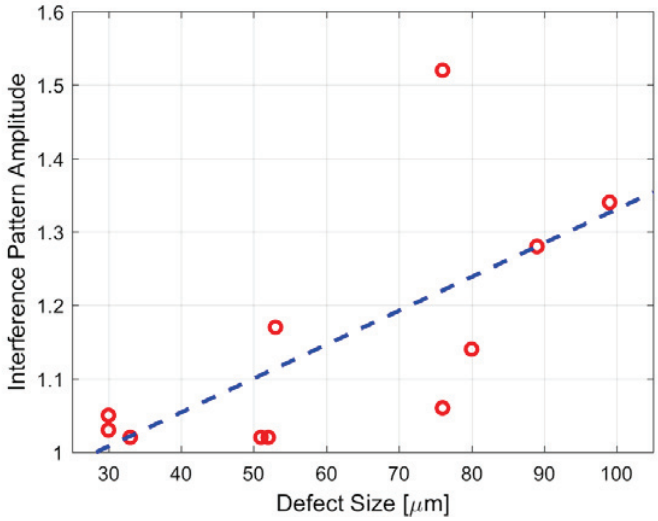

FIGURE 12. Amplitude of interference scattered wave pattern (normalized with incident wave), against optically measured defect size (perpendicular to incident wave, indent and cracks combined); dashed line: linear fit to measured amplitude values.

CONCLUSIONS

Guided wave scattering in monocrystalline silicon wafers was studied experimentally. The A_0 guided wave mode was excited selectively using a custom-made contact wedge transducer at a center frequency of 5 MHz. The scattered guided wave field around artificial surface defects was measured using laser interferometry. Defects were generated using a defined force to create an indent and micro-cracks. The surface defect size was measured optically using a microscope and correlated well with the indent force. The scattered guided wave field was measured with good spatial resolution in the near field of 3 defects for 4 force values. Significant scattered wave amplitude and a semi-circular interference pattern were observed for all defects close to the defect location. Consistently the scattered guided wave field was not symmetric to the incident wave field and crystallographic orientation. A significant increase of amplitude with defect size was observed, but with variations for all force levels, requiring further quantification. The sensitivity of guided waves for the detection of small surface defects in monocrystalline silicon wafers was demonstrated. Further research will be required to understand variation with defect size and to advance to process monitoring.

REFERENCES

1. A. Luque and S. Hegedus, *Handbook of Photovoltaic Science and Engineering*, Wiley, New York (2011).
2. M. Abdelhamid, R. Singh and M. Omar, "Review of microcrack detection technique for silicon solar cells", *IEEE J. Photovoltaics* **4**, 514-524 (2014).
3. M. Israil, A. Ghani and Y. Kerm, "Non-destructive microcracks detection techniques for silicon collar cells", *Phys. Sci. Int. J.* **4**, 1073-1087 (2014).
4. J. L. Rose, "Standing on the shoulders of giants-An example of guided wave inspection", *Mat. Eval.* **60**, 53-59 (2002).
5. J. S. Hall, P. Fromme and J. E. Michaels, "Guided wave damage characterization via minimum variance imaging with a distributed array of ultrasonic sensors", *J. Nondestruct. Eval.* **33**, 299-308 (2014).
6. B. Masserey, C. Raemy and P. Fromme, "High-frequency guided ultrasonic waves for hidden defect detection in multi-layered aircraft structures", *Ultrasonics* **54**, 1720-1728 (2014).
7. H. Chan, B. Masserey and P. Fromme, "High frequency guided ultrasonic waves for hidden fatigue crack monitoring in multi-layer model aerospace structures", *Smart Mater. Struct.* **24**, 025037 (2015).
8. B. Masserey and P. Fromme, "Analysis of high frequency guided wave scattering at a fastener hole with a view to fatigue crack detection", *Ultrasonics* **76**, 78-86 (2017).
9. B. Masserey and P. Fromme, "In-situ monitoring of fatigue crack growth using high frequency guided waves", *NDT&E Int.* **71**, 1-7 (2015).
10. M.-K. Song and K.-Y. Jhang, "Crack detection in single-crystalline silicon wafer using laser generated Lamb wave", *Adv. Mater. Sci. Eng.* **2013**, 950791, (2013).
11. S. K. Chakrapani, M.J. Padiyar and K. Balasubramaniam, "Crack detection in full size Cz-Silicon wafers using Lamb wave air coupled ultrasonic testing", *J. Nondestruct. Eval.* **31**, 46–55 (2012).
12. C. Rouge and P. Fromme, "Directivity of guided ultrasonic wave scattering at notches and cracks", *J. Phys.: Conf. Ser.* **269**, 012018 (2011).
13. H. J. Maris, "Enhancement of heat pulse in crystal due to elastic anisotropy", *J. Acoust. Soc. Am.* **50**, 812-818 (1971).
14. B. I. S. Murat, P. Khalili and P. Fromme, "Scattering of guided waves at delaminations in composite plates", *J. Acoust. Soc. Am.* **139**, 3044-3052 (2016).
15. K. Y. Kim, K.C. Bretz, A.G. Every and W. Sachse, "Ultrasonic imaging of the group velocity surfaces about the cubic axis in silicon", *J. Appl. Phys.* **79**, 1857-1863 (1996).
16. B. Audoin, C. Bescond and M. Deschamps, "Measurement of stiffness coefficients of anisotropic materials from pointlike generation and detection of acoustic waves", *J. Appl. Phys.* **80**, 3760-3771 (1996).
17. C. Prada, D. Clorennec, T.W. Murray and D. Royer, "Influence of the anisotropy on zero-group velocity Lamb modes", *J. Acoust. Soc. Am.* **126**, 620-625 (2009).
18. M. Veidt and W. Sachse, "Ultrasonic point-source/point-receiver measurements in thin specimens", *J. Acoust. Soc. Am.* **96**, 2318-2326 (1994).
19. M. Pizzolato, B. Masserey, J.-L. Robyr and P. Fromme, "*Guided ultrasonic wave beam skew in silicon wafers,"* AIP Conf. Proc., **1949**, 090005 (2018).
20. M. Lauper, P. Fromme, J.-L. Robyr and B. Masserey, "*Silicon wafer defect detection using high frequency guided waves,"* Proc. SPIE 10600, 106000G (2018).
21. P. Fromme, M. Pizzolato, J.-L. Robyr and B. Masserey, "Lamb wave propagation in monocrystalline silicon wafers", *J. Acoust. Soc. Am.* **143**, 287-295 (2018).